

# Preliminary Geological Assessment of the Northern Edge of Ultimi Lobe, Mars South Polar Layered Deposits

Bruce Murray

*Division of Geological and Planetary Science, California Institute of Technology, MS 150-21, 1200 East California Boulevard, Pasadena, California 91125*  
E-mail: [bcm@gps.caltech.edu](mailto:bcm@gps.caltech.edu)

Michelle Koutnik

*Department of Earth and Space Sciences, University of California, Los Angeles, 595 Charles Young Drive East, Los Angeles, California 90095-1567*

Shane Byrne

*Division of Geological and Planetary Science, California Institute of Technology, MS 150-21, 1200 East California Boulevard, Pasadena, California 91125*

and

Laurence Soderblom, Kenneth Herkenhoff, and Kenneth L. Tanaka

*U.S. Geological Survey, 2255 North Gemini Drive, Flagstaff, Arizona 86001*

Received November 30, 2000; revised April 20, 2001

We have examined the local base of the south polar layered deposits (SPLD) exposed in the bounding scarp near 72°–74°S, 215°–230°W where there is a clear unconformable contact with older units. Sections of layering up to a kilometer thick were examined along the bounding scarp, permitting an estimate of the thinnest individual layers yet reported in the SPLD. Rhythmic layering is also present locally, suggesting a similarly rhythmic variation in environmental conditions and a recorded climate signal at least in some SPLD strata. Locally, angular unconformities may be present, as has been reported for the north polar layered deposits (NPLD) and may likewise imply intervals of subaerial erosion in the SPLD. The outcropping layers display a broad range of weathering styles and may reflect more diverse conditions of depositions, erosion, and diagenesis than might have been expected from simple aeolian deposition modulated only by astronomically driven climatic fluctuations.

An unexpected finding of our study is the presence of locally abundant small pits close to the bounding scarp. These quasi-circular, negative, rimless features probably originated as impact craters and were modified to varying degrees by local endogenic processes, as well as locally variable blanketing. A nominal exposure age for the most heavily cratered region in our study area is about 2 million years, and the crater statistics appear consistent with those for the overall SPLD, although there are large uncertainties in the absolute ages implied by the crater size–frequency statistics, as in all martian crater ages.

Another new finding is the presence of mass wasting features along the steepest portion of the retreating bounding scarp as well as a number of examples of brittle fracture, consistent with large-

scale slumping along the bounding scarp and probably also ancient basal sliding. Both subhorizontal and high angle faults appear to be exposed in the bounding scarp, but the dips of the faults are poorly constrained. These fractures, along with the relatively undeformed layers between them, suggest to us that whatever horizontal motion may have taken place outward from the central cap region was accomplished by ancient basal sliding rather than large-scale glacial-like flow or ice migration by differential ablation, as proposed recently for the northern permanent cap and underlying NPLD. We have also obtained the first direct estimate of the regional dip of the SPLD, around 2–3° outward (northward) in one area. © 2001 Elsevier Science

**Key Words:** Mars, surface; geological processes.

## 1. INTRODUCTION

The polar layered deposits (PLD) have been regarded as key to the climatic history of Mars ever since their discovery by Mariner 9 in 1972. But that expectation has proven most difficult to realize. Now, fortunately, very large, high-resolution data sets from Mars Global Surveyor (MGS) are becoming available so there is new optimism about gaining major understanding of Mars' polar history and processes. As part of broader MGS-based systematic studies of the south PLD (SPLD), this paper presents new MGS results concerning a well-exposed part of the base of that stratigraphic section.

### a. *The Puzzling Record of the Martian Polar Deposits*

The Mariner 9 Orbiter mission revealed extensive deposits of delicately layered sedimentary material encircling and underlying the permanent polar caps. These PLD were immediately suggestive of global climate fluctuations and aeolian deposition. An extensive literature was generated speculating about how CO<sub>2</sub> solid/vapor regulation of global atmospheric pressure (Leighton and Murray 1966) could be modulated by perturbations in eccentricity and especially obliquity (Ward 1974, 1979, Murray, Ward, and Yeung 1973). Such analyses led to suggestions that the individual layers recognized in the PLD somehow correspond primarily to obliquity-driven climatic cycles of 10<sup>5</sup> to 10<sup>6</sup> years. Mariner 9 provided only limited coverage of the north polar layered deposits (NPLD), leading to a presumed symmetry in polar climate history and a correlated polar “layercake” stratigraphy of the PLD recording global climate fluctuations (Murray *et al.* 1972, Soderblom *et al.* 1973, Cutts 1973).

Large-scale differences between the northern and southern polar deposits became evident quickly, such as the higher altitude and generally older (Noachian) underlying rocks of the south as well as the much larger residual cap in the north. The Viking Orbiters starting in 1976 greatly improved the resolution and coverage in the north as well as enhancing the southern coverage. A significant revision of ideas ensued. It became evident that the conspicuous dark bands in the north were often asymmetric troughs rather than scarps, as had been the common interpretation of the southern features (e.g., Dzurisin and Blasius 1975). Unconformities were also recognized in the NPLD, arguing against simple “layercake” stratigraphy (Cutts *et al.* 1976, Blasius *et al.* 1982, Howard *et al.* 1982a,b). Recently, the MGS Mars Orbiter laser altimeter (MOLA) has provided detailed topographic descriptions of the northern permanent cap and its characteristic troughs, leading to competing flow-based as well as ablation-dominated models of their formation (Zuber *et al.* 2000, Ivanov and Muhleman 2000a, Fisher 2000). MOLA data, however, as well as newly processed Viking stereo imagery (Schenk and Moore 1999), show that the exterior parts of the southern PLD exhibit mainly equatorward-facing scarps rather than troughs, although the central region does exhibit troughs (Ivanov and Muhleman 2000b).

The central regions of both permanent caps are dome-shaped (Ivanov and Muhleman 2000b) even though the permanent cap is not symmetrical about the pole in the south. Thus, the two polar regions differ profoundly not only in regional height, but also in regional morphology and the geographical extent of the permanent cap. Furthermore, the southern rather than the northern permanent cap proved to be the site of excess solid CO<sub>2</sub> required for continuing CO<sub>2</sub> solid–vapor balance on Mars (Farmer *et al.* 1976, Kieffer 1979, Paige *et al.* 1990). Plaut *et al.* (1988) argued that the crater density on the SPLD suggests an average surface age of at least 120 million years, significantly older than previously thought. The cratering flux assumed by Plaut *et al.* (1988) was reinterpreted to be unrealistically low by Herkenhoff and Plaut (2000) who suggested that the average SPLD surface age is

5–20 million years. The surfaces of the NPLD are clearly much younger (less than 100,000 years) because no impact craters greater than 300 m in diameter have been confidently identified (Cutts *et al.* 1976, Herkenhoff and Plaut 2000). The exposed SPLD appear considerably older than the NPLD, with a mean surface age of many obliquity time scales (Herkenhoff and Plaut 2000), even allowing for chaotic orbital interactions (Touma and Wisdom 1993).

The increasing recognition of differences between the two caps has progressively made a straightforward global alternation in aeolian deposition of suspended sediment between the two poles (driven by obliquity and eccentricity changes) a less likely explanation, though it once seemed so appealing. However, a new paradigm has not yet emerged to explain the rapidly growing body of information.

Our working hypothesis for this study is limited to the exterior SPLD and presumes (1) that the layers include some, but not necessarily solely aeolian, deposits, (2) that a climate signal may be included, but drivers other than obliquity and eccentricity may also be recorded, and (3) outward motion of the sedimentary stack, if it has happened at all, has been accomplished by basal sliding, not glacial-like flow or ablation. We intend to sharpen this hypothesis in this investigation, or modify it appropriately. Integration of a theory of the full SPLD and the small permanent cap is not attempted here, much less a global reconciliation of the north and south polar regions.

### b. *Scope and Approach*

We address the SPLD and focus on the base of the stratigraphic section where there is a well exposed basal contact suitable for addressing the above questions of ice-based movement and deformation and for examining the characteristics of exposed layers. The latitudes between 72° and 76°S encompass a dissected plateau of layered deposits from 170° to 230°W longitude known as the Ultimi lobe (Vasavada *et al.* 2000, Tanaka and Scott 1987). This label was derived from the previous description of Ultimi Cavi given by Condit and Soderblom (1978). The specific focus of this study is the northern edge of the Ultimi lobe, 72°–74°S and 215°–230°W. Figure 1 provides the context for most of this study, including a regional image mosaic, a geological sketch map, and the locations of MGS Mars Orbiter Camera (MOC) narrow-angle (NA) footprints.

### c. *Stratigraphic Setting of This Study*

The sharp, unconformable and undisturbed contact of the SPLD with an underlying massive unit is well exposed in Figs. 2 and 12. The underlying massive unit exhibits large characteristic pits suggestive of collapse and/or ablation, similar to those observed elsewhere in the south polar region (Sharp 1973, Plaut *et al.* 1988), and has been mapped as Hesperian in age (Tanaka and Scott 1987, Plaut *et al.* 1988). In the first Mariner 9 descriptions of the south polar region, this underlying unit was

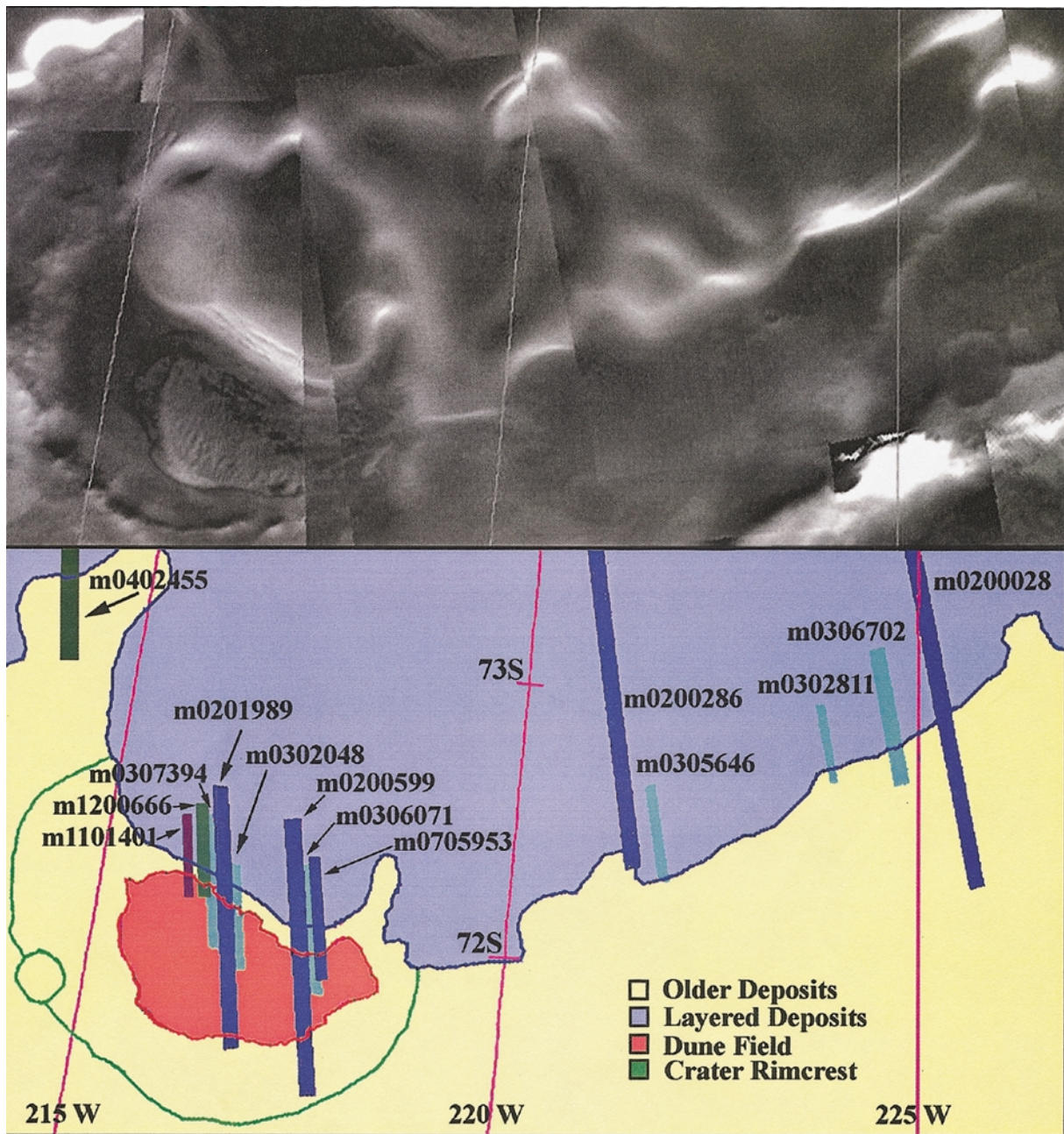


**FIG. 1.** Top: Northern edge of Ultimi lobe of SPLD, roughly 72°–74°S, 215°–230°W, displayed with MOC wide angle (WA) context mosaic superposed on Viking image mosaic. MOC WA mosaic is about 250 km wide; south is at the top and range of  $L_s = 149$ – $192^\circ$ . Solar illumination is from the lower right. Bottom: Interpretative geologic sketch map of mosaic. Thin blue line denotes bounding scarp of south polar layered deposits. MOC NA footprints of images discussed in text displayed as colored rectangles.

referred to as the “Etched and Pitted Terrain” (Murray *et al.* 1972). Significantly, in Figs. 2 and 12 the SPLD contact buries an unfilled preexisting pit in the underlying unit. This indicates that the episode of pitting occurred before the formation of the SPLD, likely under different environmental conditions than subsequently, and suggests an extensive depositional hiatus (see Tanaka and Kolb, this volume, Plaut *et al.* 1988).

In addition, the pits are not filled or buried by dunes composed of sand-size particles that hypothetically might have weathered out of the retreating scarp. This might be considered indirect confirmation of the notion that the SPLD are composed of water ice and dust only and suggests that the retreating bounding scarp is undergoing aeolian deflation at present. These observations stand in sharp contrast to the relations observed between the

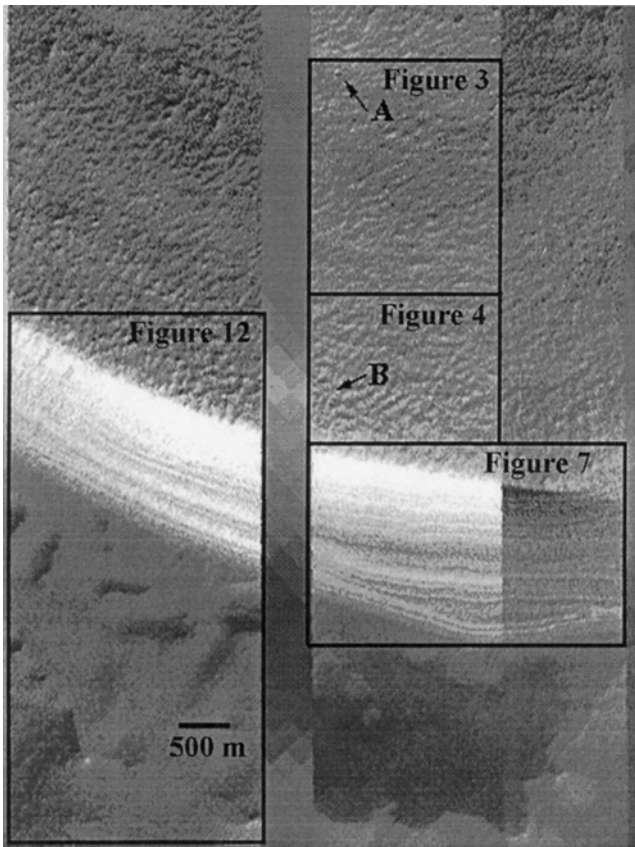


**FIG. 2.** Portions of MOC NA m0200599, m0306071, and m0705953 at 72°S, 217°W as viewed in Mars polar-stereographic GIS (Geographic Information System) with south at the top. Illumination is from the lower right with solar elevation angles of 0.6° (m0200599), 12° (m0306071), and 26° (m0705953). Outlines of Figs. 3, 4, 7, and 12 shown. Sharp lower contact with underlying massive, pitted unit is apparent. Thickness of this layering of layered deposits is about 700 m. Features denoted by A and B are discussed below in relation Figs. 3 to 4 s and respectively.

very prominent circum-polar sand erg and the PLD in the north (Thomas and Weitz 1989).

The exposed quasi-horizontal upper surface of the SPLD that comprises the Ultimi lobe has been extensively studied and described in association with the selection of the Mars Polar Lander (MPL) landing site (Vasavada *et al.* 2000) and with the MOC follow-up studies (Malin and Edgett 2000). The MOC NA coverage was concentrated around the targeted MPL site at 76°S, 195°W, which is adjacent to our study area and exhibits the same kind of textured surface of the SPLD that we find. Those MPL images reaffirm the earlier impression that the SPLD are quasi-horizontal. In Fig. 8 we estimate that the regional slope specifically is 2–3 degrees northward. We generally assume comparably low dips away from the pole in the Ultimi lobe. Generally a single layer crops out over a large area, with exposed stratigraphic sections visible only at scarps or local slopes. The hypothesis that the SPLD likely have a high water ice content has been reinforced recently by Smith *et al.* (1999) based upon MGS gravity and MOLA data.



**FIG. 12.** The lower portion of MOC NA frame m0200599, as shown in Fig. 2.  $L_s = 151.3^\circ$ ; resolution = 5.7 m/pixel; illumination is from the lower right. The line cutting through the image indicates that the region below was preferentially stretched to bring out detail within pitted features. Note the sharp contact of the SPLD with the exposed underlying massive unit featuring unfilled characteristic large pits on its surface, which is determined to be level from MOLA data. The pitted unit passes smoothly under the SPLD with no evidence of disruption due to hypothetical ice movement (see also Fig. 7b). Indeed, some of the pits appear to extend under the SPLD, arguing for an extended period of subaerial exposure before the beginning of SPLD deposition. In the lowest portion of the image, layering in the underlying unit is exposed in a second scarp denoted by arrows.

At MOC resolution, a characteristic ridged and gullied texture is common over large areas, usually exhibiting a locally linear alignment along with occasional local dunes and perhaps other blanketing. This rough surface was completely unexpected before MGS, has no reported terrestrial analog, and remains unexplained. Malin and Edgett (2000) estimated slopes generally less than  $10^\circ$  and with relief less than 5 m in the vicinity of the targeted landing site. Similarly, Herkenhoff and Kirk (2001) found very low slopes on the Ultimi lobe.

Our working hypothesis about this upper surface of the SPLD in our study area is that it is generally in a state of long-term ablation and erosion, which has resulted in the characteristic ridge and gully terrain. The terrain develops a consistent morphology regardless of which layer is exposed at the surface, suggesting no significant differences in mechanical properties among the near-surface layers.

## 2. DATA AND ANALYSIS TECHNIQUES

We have used primarily the MOC images with an  $L_s$  range of  $151^\circ$ – $192^\circ$  corresponding to when the area was generally

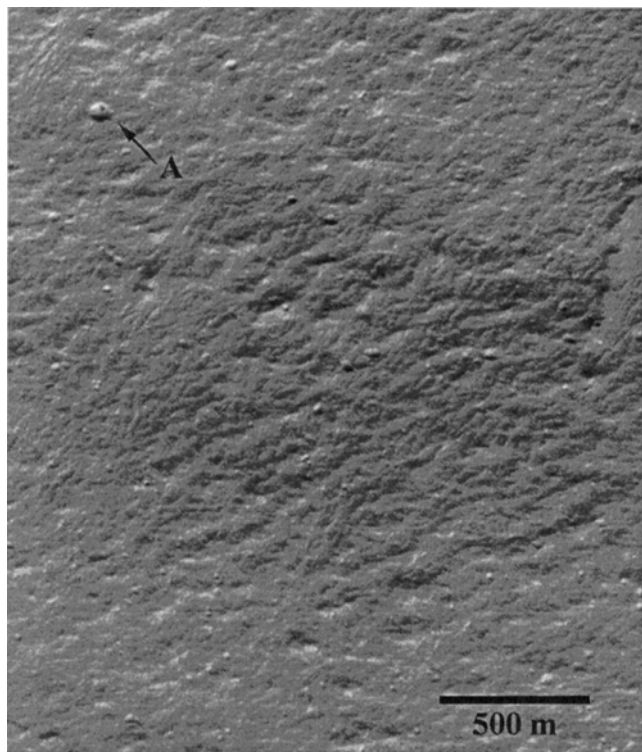


**FIG. 3.** Top portion of MOC NA frame m0306071, as indicated in Fig. 2. Illumination is from the bottom right; resolution = 3.6 m/pixel. The feature denoted 'A' serves as a reference point for the context image (Fig. 2) and as a prominent example of near-circular depression. Many other smaller craters of varying degrees of circularity are visible in the original image. The texture of the residual surface has a relief of approximately 5 m at the MPL landing site 400 km distant on a very similar appearing residual surface (Malin and Edgett 2000). Taken during spring season, the surface is covered by seasonal  $\text{CO}_2$  frost.

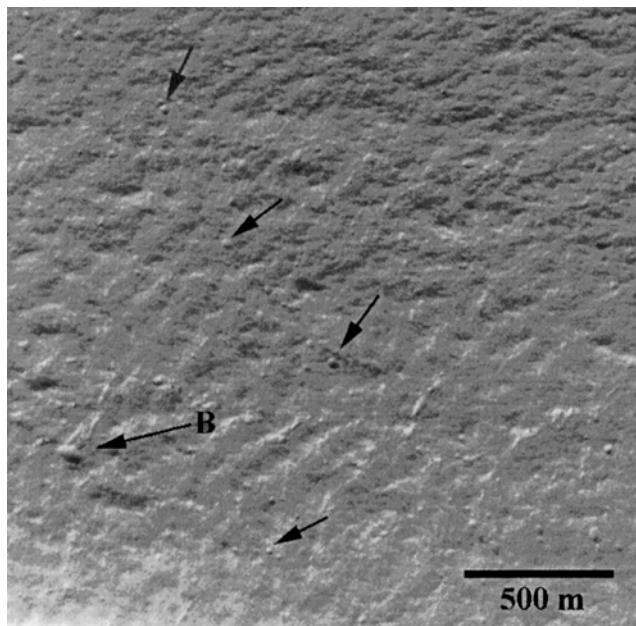


**FIG. 4.** Lower cratered region of MOC NA frame m0306071, as indicated in Fig. 2. Illumination is from the bottom right; resolution = 3.6 m/pixel. The feature denoted 'B' serves as a reference point for the context image (Fig. 2); note the elongate nature of this feature in comparison to other circular features designated by arrows. Both Figs. 3 and 4 display a spectrum of crater-like forms ranging from circular to elongate.

covered by seasonal  $\text{CO}_2$  frost, from the end of south polar winter through the beginning of south polar spring. These included mainly early MGS mapping phases 2, 3, and 4. We have also used a few MOC images from later mapping phases 7–12. These images have an  $L_s$  of approximately  $200^\circ$ – $307^\circ$ , corresponding to the beginning of southern spring and moving into summer seasonal conditions. Table I shows a complete list of all images used in this study and associated image statistics. We also used the extensive MOLA data available from the MOLA website (<http://ltpwww.gsfc.nasa.gov/tharsis/mola.html>) as of September 2000.

The image data were processed using the Integrated Software for Imagers and Spectrometers (ISIS) developed by the United States Geological Survey (USGS), adapted specifically to support the processing of MOC images.

We processed the MOLA data and used the spacecraft clock times to match the individual MOLA points to line numbers in the narrow angle images. The time at which each line was exposed is known from the start time of the image and the line exposure duration, which are recorded in the Planetary Data System (PDS) header. In the sample direction, the position of the MOLA ground track was determined by use of estimates provided from other workers (Anderson, Ivanov, Malin, and Soderblom, personal communication, 2000). The three estimates were all at a sample number of  $1575 \pm 50$  out of the full 2048 samples on the CCD (Charge Coupled Device). This was converted to a sample number on the image by taking into consideration the cross-track

TABLE I  
Ultimi Lobe MOC Image Data

Image number	Ls	Resolution (m/pixel)	Aspect ratio	Summing	Incidence angle	Center latitude	Center longitude	Width (km)
ab109503	256.95	14.37	1.5	1	49.96	-74.19	212.81	29.59
m0200599	151.28	5.51	1.06	4	89.36	-71.88	217.55	2.83
m0201989	155	5.51	1.86	4	88.11	-72	216.59	2.83
m0302048	169.24	1.38	1.85	1	82.65	-72	216.74	1.06
m0302811	170.94	1.38	1.86	1	82.64	-72.84	223.84	1.07
m0305646	178.92	2.76	1.06	2	79.13	-72.48	221.76	1.42
m0306071	180.07	2.76	1.59	2	78.29	-72	217.64	2.13
m0306702	181.82	4.13	1.06	3	78.31	-72.94	224.63	2.79
m0307394	184.15	2.75	1.59	2	76.71	-72.12	216.37	2.12
m0402455	192.45	2.76	1.59	2	74.28	-73.43	213.59	2.13
m0705953	215.9	2.76	1.06	2	64.02	-72.07	217.65	2.84
m1101401	279.89	1.38	1.6	1	50.88	-72.23	216.17	1.06
m1200666	296.25	1.38	1.6	1	52.52	-72.26	216.24	1.42

TABLE II  
Ultimi Lobe Crater Data

Count number	Diameter (m)	Count number	Diameter (m)	Count number	Diameter (m)
1	16.01	38	23.56	75	31.45
2	16.05	39	23.56	76	31.54
3	16.49	40	23.56	77	31.67
4	16.6	41	23.68	78	31.84
5	16.74	42	23.7	79	31.87
6	16.78	43	23.7	80	32.33
7	16.92	44	23.75	81	32.96
8	16.93	45	23.81	82	32.99
9	17.18	46	23.82	83	33.33
10	17.89	47	23.95	84	33.43
11	17.96	48	23.96	85	33.56
12	18.77	49	24.1	86	33.57
13	19.08	50	24.1	87	33.93
14	19.18	51	24.1	88	34.02
15	19.44	52	24.39	89	34.72
16	19.45	53	24.39	90	35.45
17	19.45	54	25.32	91	35.45
18	19.63	55	25.42	92	35.45
19	19.93	56	25.52	93	35.45
20	19.97	57	25.74	94	35.62
21	20.08	58	25.88	95	35.81
22	20.14	59	26.59	96	35.83
23	20.45	60	26.78	97	35.91
24	21.14	61	26.78	98	36.35
25	21.14	62	26.8	99	37.45
26	21.16	63	27.11	100	37.45
27	21.85	64	27.17	101	38.15
28	22.02	65	27.28	102	38.26
29	22.17	66	27.3	103	38.32
30	22.62	67	28.48	104	41.48
31	22.63	68	29.61	105	42.32
32	22.65	69	29.81	106	45.48
33	23.1	70	29.94	107	48.07
34	23.34	71	30.01	108	56.01
35	23.34	72	30.19	109	58.51
36	23.41	73	30.78	110	61.39
37	23.56	74	30.78	111	82.72

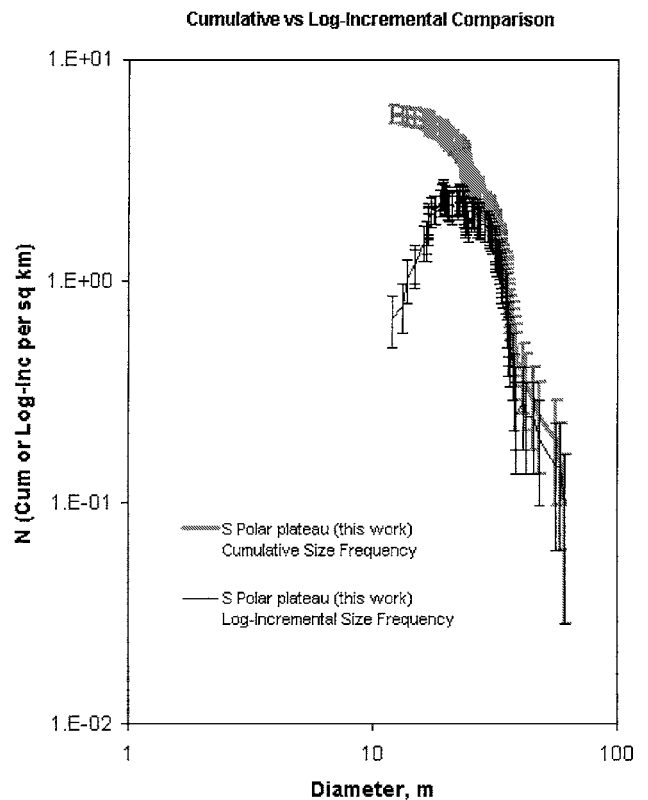


FIG. 5. Crater size–frequency distribution for the heavily cratered portion of Fig. 2. The sample area encompasses the width of both m0200599 and m0306071, a 20.7 km<sup>2</sup> area from the edge of the scarp to the end of the heavily cratered area (southward) in these images. The surface shows the highest abundance of crater pits for the region studied in this work. Two methods of displaying the data (cumulative and log-incremental size frequency distributions) are compared.

summing and the offset of the image from the edge of the CCD during acquisition. This  $\pm 50$  pixels is less than the size of the MOLA footprint, so any residual error was not significant.

The GIS package ArcView, adapted at Caltech for Mars Polar Stereographic projection, enabled us to load in different data sets for combined viewing. The ArcView project we use consists of a background map composed of Viking images (MDIM), wide angle (WA) MOC context image mosaics of select regions, MOC footprints (place locators for each MOC image), processed MOC NA images, and shaded relief topographic maps of the MOLA data. The ability to see where the images lie in relation to each other and in what topographic context allows for the maximum understanding from these two data sets.

### 3. CRATERS

#### a. Morphologies of Individual Features

A zone adjacent to the bounding scarp in this study shows an area of an unusually high abundance (for the SPLD) of small rimless pits that we suspect are impact craters. However, definitive morphological evidence for the origin of these  $\sim 16$  to  $\sim 83$  m, quasi-circular negative features generally is lacking. Examples of these features are shown in Figs. 3 and 4. They lack the raised rims expected of primary impact craters, and the alignments and parallel, oriented shapes characteristic of secondary crater chains, and flat floors, aligned shapes, and coherent regional associations that might suggest an endogenic origin. Furthermore, there are many fresh-appearing quasi-circular craters that occur on top of and around the strongly ridged texture of the residual surface with a seemingly random distribution. This would suggest an exogenic origin for them, and subsequent to the endogenic processes that formed the ridged terrain itself.

Rarely, individual layers exposed in scarps do exhibit a slightly pitted weathering style. Hence at least some of the SPLD strata are capable of eroding into pitted forms, at least on exposed scarps, but we cannot connect the topmost residual layer to any such pattern. In the face of inconclusive high-resolution morphological evidence, we have examined the size–frequency distributions and the areal distribution patterns and characteristics for further clues.

#### b. Crater Statistics

Impact crater statistics were tabulated for the plateau of the layered terrain that exhibits the highest crater density in the study area, part of which is shown in Figs. 3 and 4. This area of  $20.7 \text{ km}^2$  covers the full width of MOC NA frames m0200599 (approximately lines 2900–3600) and m0306071 (approximately lines 2200–3300). Relevant statistics on these images can be found in Table I. All quasi-circular, negative features were tabulated by location and average diameter. This resulted in a population of 111 putative craters for a  $20.7 \text{ km}^2$  area that range from  $\sim 16$  to  $\sim 83$  m in diameter. The complete data set of crater diameters tabulated is listed in Table II. Smaller craters are also present

but cannot be measured reliably. No larger ones are present in the selected area. The data from Table II are plotted in both cumulative and log-incremental size frequency as functions of crater diameter in Fig. 5. The cumulative size–frequency distribution is the number of craters per unit area of diameter greater than  $D$ , e.g., integrated from  $D$  to  $\infty$ . The log-incremental size–frequency distribution is the number of craters per unit area with diameters between  $D$  and  $\sqrt{2} D$  (cf. Hartmann *et al.* 1981). Hartmann (1999) argues that the log-incremental plot better shows the structure as variations from bin to bin whereas the cumulative plot is a “running sum” and therefore does not show as much structure. The drawback is that it also strongly enhances noise due to weak statistics. In any case we use the log-incremental version to facilitate comparison with crater population isochrons for Mars modeled by Hartmann (1999).

Figure 6 compares the crater size frequency of the polar plateau region studied here (area  $\sim 20.7 \text{ km}^2$ ) with that for nearly the entire exposed south polar layered terrain complex (area  $\sim 21.11 \times 10^6 \text{ km}^2$ ), compiled by Plaut *et al.* (1988), along with model isochrons from Hartmann (1999). Hartmann’s model

**Polar Plains Craters vs Hartmann (1999) Isochrons**

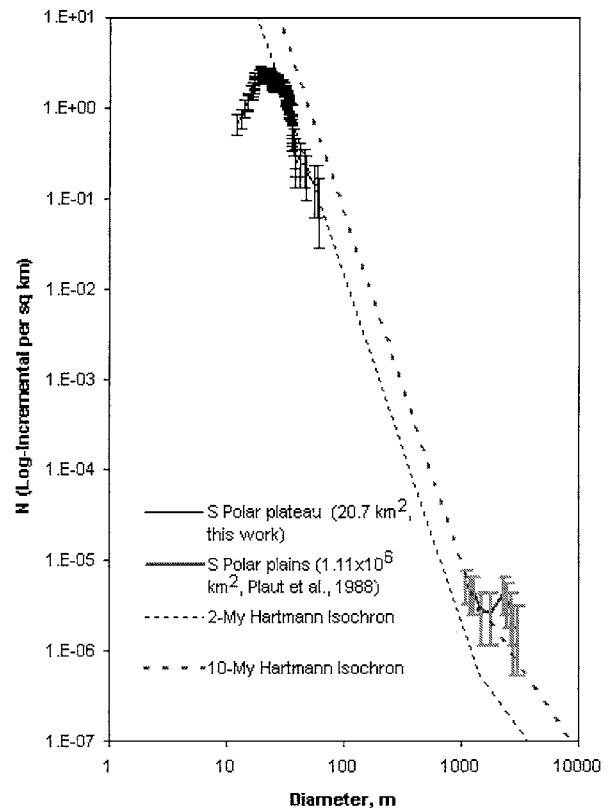


**FIG. 6.** Log-incremental size frequency distribution for the small polar plateau area (see Figs. 2, 3, and 4) compared with that for the entire south polar layered deposit complex from Plaut *et al.* (1988). Fitted through both distributions are model isochrons developed by Hartmann (1999) in log-incremental format. The  $\sim 10$ -Ma model age for the whole south polar layered terrain complex is consistent with the production model of Herkenhoff and Plaut (2000).

uses a scaling between the impact-crater-production rate during the last few billion years (following cessation of postaccretionary heavy bombardment) for Mars of 1.6 times that for the Moon ( $R = 1.6$ ), with an uncertainty of  $+1.6/-1.0$ . This value is consistent with values from Shoemaker and Helin (1977) ( $R = 1.8$ ), based on astronomically observable asteroids and comets, and from Soderblom (1977) ( $R = 1.5$ ), based on the range of cratering populations found on volcanic plains on Mars, the Moon, and Mercury. Herkenhoff and Plaut (2000) modeled the Plaut *et al.* (1988) data assuming  $R = 2$  to derive an average age of the south PLD of  $14.5 \pm 7.2$  million years. On the basis of other studies that suggest an increased cratering flux during the past few 100 million years, Herkenhoff and Plaut (2000) also considered a higher cratering rate ( $R = 4$ ) that implies an average age of only  $7.25 \pm 3.6$  Ma. We recognize that this topic remains an area of active research (Neukum and Ivanov 2001). In addition, Herkenhoff and Plaut (2000) modeled the SPLD crater population as resulting from a vertical resurfacing (erosional and/or blanketing) process that removed craters at a steady rate proportional to crater depth (Plaut *et al.* 1988).

They found that resurfacing rates of  $60 +18/-23$  m/million years for  $R = 2$  and  $120 +36/-46$  m/million years for  $R = 4$  are consistent with the observed craters larger than 1 km in

diameter. Despite the large uncertainties in the recent cratering flux on Mars, the exposure ages of the small area studied here can be compared in a relative sense to the rest of the SPLD, as detailed in the next section.

The Hartmann isochrons plotted in Fig. 6 show two distinct branches above and below about 1400 m diameter. As Hartmann (1999) notes, the branch above this diameter (slope  $\sim -1.8$ ) is believed by all workers to directly reflect the “primary” flux, that is the impact flux of bolides directly from space (cometary and asteroidal fragments). Below this diameter is the so-called “secondary” branch (slope  $\sim -3.8$ ), which is generally agreed (originally argued by Shoemaker 1965) to have arisen from comminution (breakup) of material involving impact of bolides from the primary population. This “breakup” can occur during collisions within the asteroid/comet debris swarms or can be due to gravitational separation or to atmospheric breakup on entry, or it can be produced at the planet’s surface in the form of secondaries flung widely around the planet. The details have been long argued. The truth may involve all these processes to some extent. This “secondary” branch on Mars is likely a mixture of far-flung “background” secondaries from primary impacts and from a steep-power function distribution of fragments produced by collisions among the source space debris.

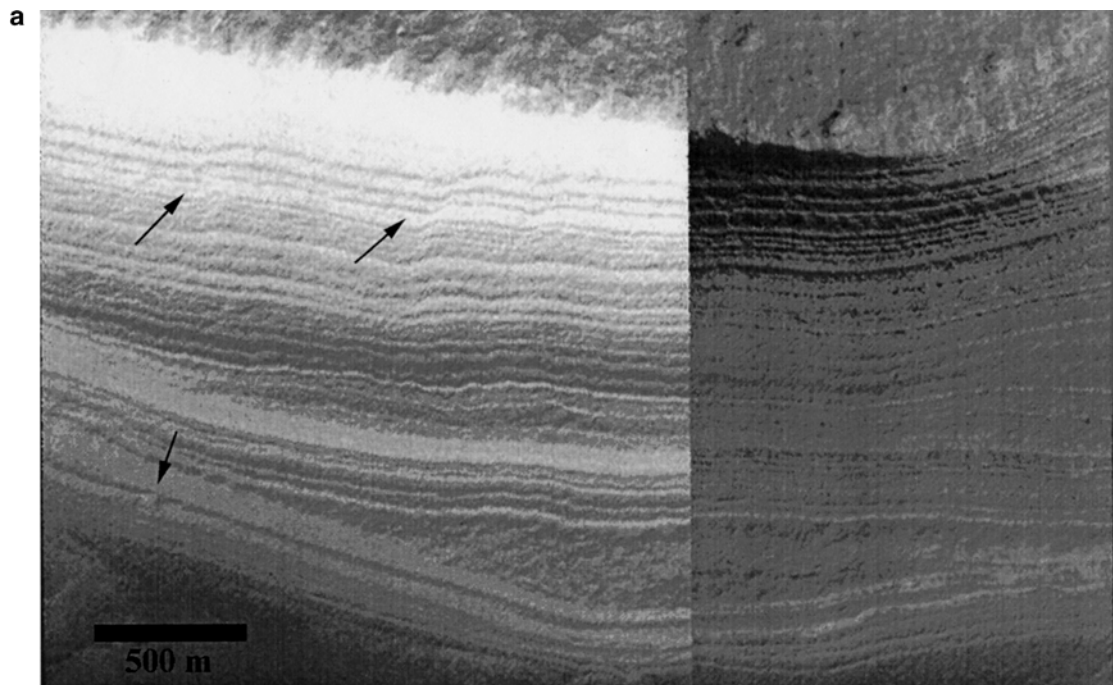


**FIG. 7a.** Close-up view of the layered region outlined in Fig. 2. Left: MOC NA frame m0306071 taken at  $L_s = 180.7^\circ$ ; resolution = 3.6 m/pixel, illumination is from the bottom right. Right: MOC NA m0705953 taken at  $L_s = 215.9^\circ$ ; resolution = 2.9 m/pixel, illumination is from the bottom right. Vertically disturbed layering, indicated by arrows, and evident at multiple locations, may be incipient faulting. The wedge-shaped feature may be a local unconformity, but a topographic origin is more likely. The difference in contrast across the two images is due to sublimation of seasonal frost during time between image acquisitions. Each has been independently contrast-stretched for maximum discriminability of layers. Small craters are visible at the top of the image above the layered exposure. Note the sharp contact between the SPLD and the underlying unit. Across this section of about 600 m thickness there are approximately 55 individual layers.

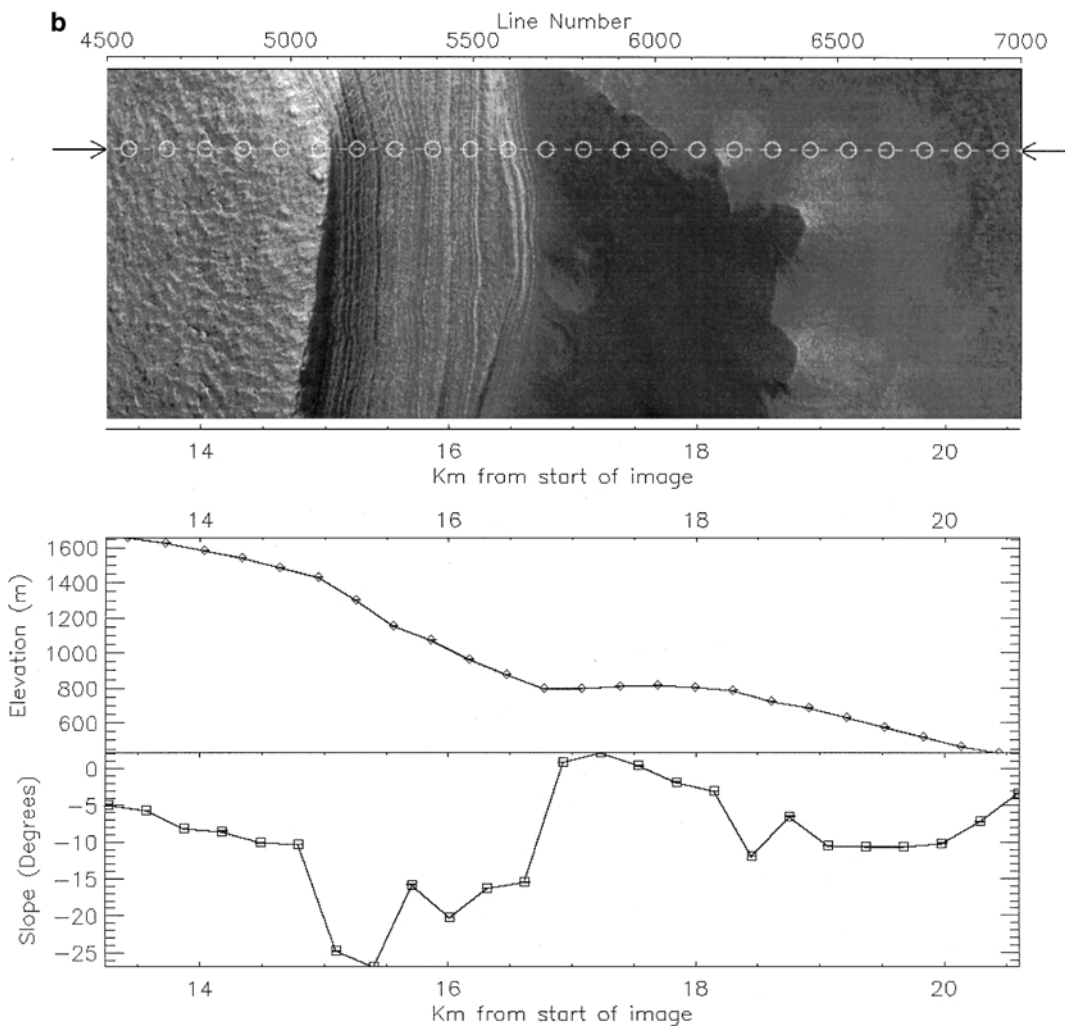


FIG. 7b. MOLA track in image m0705953 showing elevation and slope profiles. The maximum slope over this region is approximately  $24^\circ$  over an elevation change of about 600 m. The upper residual surface steepens in northward dip in the extension of this profile to the left (southward).

### c. Surface Age

Isochrons from Hartmann (1999) nominally indicate model ages for this unit on the order of 2 Ma and about 10 Ma for the entire south polar layer complex based on data from Plaut *et al.* (1988). The latter age is similar to the surface ages estimated by Herkenhoff and Plaut (2000) using a different model for the recent cratering flux on Mars. The slope of the isochrons at the smallest crater sizes is poorly constrained by observations of martian craters, and their vertical positions are uncertain by at least a factor of 2 (Hartmann 1999). It is therefore difficult to accurately compare the modeled surface ages of this study area and the rest of the SPLD, but the Hartmann (1999) production model suggests that the study area is somewhat younger than the average SPLD. Alternatively, the observed crater population may be modeled as the result of steady-state cratering and resurfacing (erosional or depositional) processes (Plaut *et al.* 1988, Herkenhoff and Plaut 2000). The crater size–frequency distribution in the study area may be consistent with the popula-

tion of larger craters throughout the SPLD (Plaut *et al.* 1988) if steady-state resurfacing has occurred. Such modeling is the subject of ongoing research and is not reported here. Cratered surfaces on the SPLD outside the study area, which are deficient in 20–80 m craters compared to our study area, may have been eroded or buried within the past 2 million years, consistent with the resurfacing rates of 40–150 m/Myr modeled by Herkenhoff and Plaut (2000). The craters within the study area are probably only a few meters in depth and would have been completely eliminated at such resurfacing rates in less than 100,000 years. Therefore, the study area appears to have been much less affected by the resurfacing processes that appear to have modified most of the SPLD.

### d. Areal Distribution of Cratering

Secondary crater chains on SPLD surrounding the large ( $\sim 23$ -km diameter) impact crater McMurdo ( $84.5^\circ\text{S}$ ,  $0^\circ\text{W}$ ) were described initially by Howard *et al.* (1982b), and more recently

by Tanaka *et al.* (2000) and Herkenhoff (2001). Herkenhoff and Kirk (2000) also ascribe some small features at 84.7°S and 10.6°W as possibly due to the ejecta from McMurdo. However, McMurdo is located approximately 1300 km from our study site and is not a plausible source for the craters we find.

We also note that craters no larger than about 200 km in diameter seem to have formed during the Amazonian anywhere on Mars (Tanaka, 1986). Given this paucity of large Amazonian craters relative to our study area, we conclude that the observed craters in our study area most likely reflect a production function of incoming bodies and of background secondaries. Therefore, the isochron of ~2 million years can be used as a plausible estimate. It seems to us less likely that they are a secondary swarm produced by a very recent event and that there is a nearby primary that somehow escapes detection or has eroded away.

Even more complexity in the origin of these features is evident when examining the areal distribution of the craters associated with the bounding scarp. Generally the highest abundance is adjacent to the scarp itself, which then diminishes progressively moving southward (poleward). Overall it is consistent, for example, with diminished blanketing approaching the bounding scarp. Interestingly, a number of MOLA traces such as those in Fig. 13b show that the nearly level residual surface develops a gentle but increasing northward slope right up to the edge of the bounding scarp. Thus the variation in crater abundance may be the result of the nondeposition or removal of blanketing on the residual surface near the bounding scarp, perhaps associated with enhanced wind erosion associated with that prominent topographic change. Indeed, variations in the thickness of such a hypothetical blanketing layer can be invoked generally to account for the occasional abundance and general absence of small craters.

#### *e. Preliminary Interpretation of Local Cratering Record*

Any interpretation of these craters must necessarily invoke several successive processes to account for the combined morphological size–frequency data and areal distribution. We find it difficult to attribute the observations solely to an endogenic origin. In particular, the seemingly random distribution of fresh-looking circular craters across the strongly textured residual surface argues for an exogenic origin at least in part. On the other hand, endogenic modification may be required to account for the dominantly noncircular, subdued negative forms, although some workers argue the opposite (Plaut, personal communication, 2001). Our working hypothesis is that an impact population is recorded that has been subsequently modified by endogenic processes and by blanketing (or erosion), except very close to the bounding scarp. Even if some or most of the craters are not formed by impact, our crater statistics still yield a maximum age for surface modification.

## 4. LAYERING

The basal scarp, as well as other scarps higher in the section, provide striking exposures of the individual layers that make up

the SPLD. Layered sections available in the NA images are well presented in Figs. 7a, 8a, 9–11a, 13a, and 14. Specific interpretations are provided in the accompanying captions.

Many tens of layers are exposed in scarps ranging from 0.5 to 1.0 km in height. Individual strata range from over 100 m thick to the minimum detectable thickness of close to 1 m. Approximately 55 layers are discernible in the 600-m-thick section exposed in Fig. 7a, giving an average thickness there of just over 10 m. In Fig. 11a, more than 50 layers can be discerned over a nearly 500-m-thick section. Again an average thickness of about 10 m is indicated. About 35 layers can be recognized over a thickness of 800 m in Fig. 8a, suggesting an average layer

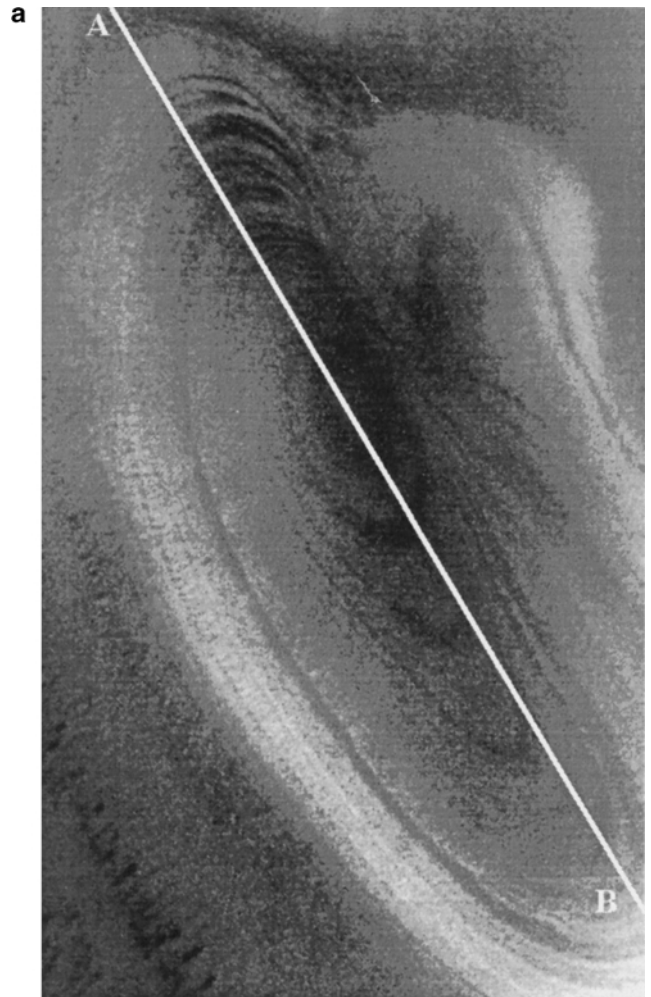


**FIG. 8a.** A portion of MOC NA frame ab109503 at 74°S, 213°W; resolution = 18 m/pixel, illumination is from the upper right. An approximately 800-m-thick sequence of about 35 layers is exposed in this 20-km-long headwall of a trough. One conspicuous dark-toned layer is visible over a wide range of solar azimuths demonstrating that it is an albedo feature. In contrast, most of the other layers reverse tone over varying solar azimuths indicating that a varying outcrop slope is the cause of the distinctive layering. The line across the image marks the location of the brightness plot, slope profile, and elevation profile as shown in Fig. 8b.

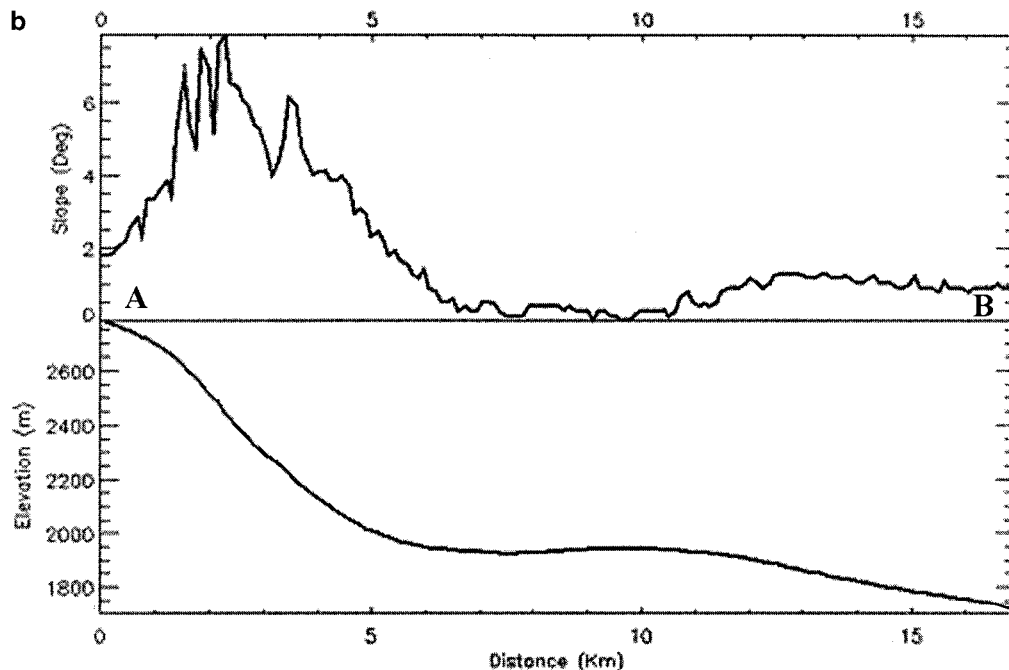


FIG. 8b. MOLA slope profile and MOLA elevation profile for MOC NA frame ab109503, located along the line drawn across the image of Fig. 8a. Note that the depression transitions to the trough at its northern end. The maximum slope across this region is near  $8^\circ$ , much shallower than at the Boundary Scarp. By measuring the height of a prominent band, we estimate the regional dip component of the layers in the profile to be about  $2\text{--}3^\circ$  in the direction  $60^\circ$  east of north, which is away from the south pole as has been expected but not demonstrated previously. Note the evidence of subtle terracing at the left end of the profile.

thickness of just over 20 m in that rather low-resolution image (18 m/pixel).

Obviously these estimates are all limited by image resolution. Thus, the true average thickness may be somewhat below the 10 m range. It is of interest to determine just how thin some of the SPLD layers are, but that quantity is difficult to estimate because the distinctive image tone denoting an individual layer can arise from either an intrinsic albedo variation, or alternatively, can be the consequence of the varying slopes of successive outcropping layers. However, when seasonal  $\text{CO}_2$  frost covers the layers (such as in Figs. 7a (left side), 9–11a, and 12), then the banding should arise only from slope variation. In Fig. 11a, the arrows point to a thin dark layer in one case and a thin bright layer in the other. Both thin layers exhibit a horizontal projection of about 10 m each. The *average* surface slope there, based on MOLA data, is about  $5.3^\circ$ . Figure 11b shows that if the layers were exposed smoothly parallel to that average slope, the thickness would be about 92 cm. In that case, the layer would appear to be the same brightness as surrounding layers that were also sloping toward the sun because seasonal frost coverage at the time this image was acquired should mask any intrinsic albedo variations leaving only layer-to-layer slope variations to create the image tones we see. However, if an exposed bed exhibited an additional  $5^\circ$  slope toward the sun, then the thickness would be about 1.8 m, and the layer should also appear slightly brighter assum-

ing Lambert scattering. An excess of slope of  $10^\circ$  would yield a thickness of 2.7 m and  $15^\circ$  excess slope would correspond to 3.7 m. Accordingly, the image suggests to us a minimum thickness layer of 1–4 m here. The thinnest layers may be no thicker than 1 m, perhaps even thinner.

The variety of textures that the individual layers display as they erode in scarp exposures is notable. The detailed erosional pattern of each layer must reflect intrinsic differences in original composition and texture imparted during deposition and/or during temporary hiatus, perhaps then modified by subsequent diagenesis. Hence, the detailed variations visible in apparent albedo, outcrop slope, and especially along-strike texture testify to a rich variation of changing physical attributes of the environment in which these deposits accumulated and were buried. Such variations exceed those implied in previous theories of origin based on presumptions that astronomically driven climatic variations on a global scale solely governed aeolian deposition for the SPLD. It seems to us that a broader range of possible depositional circumstances must be considered initially beyond simply aeolian, perhaps including elements of volcanic, impact, or periglacial processes. Or perhaps the SPLD are sensitive to shorter term climate variations and weather, such as large-scale dust-storm activity.

Many images show good lateral continuity of layers exposed in scarps over at least tens of kilometers, but some significant vertical breaks are also apparent. For example, Fig. 7a suggests

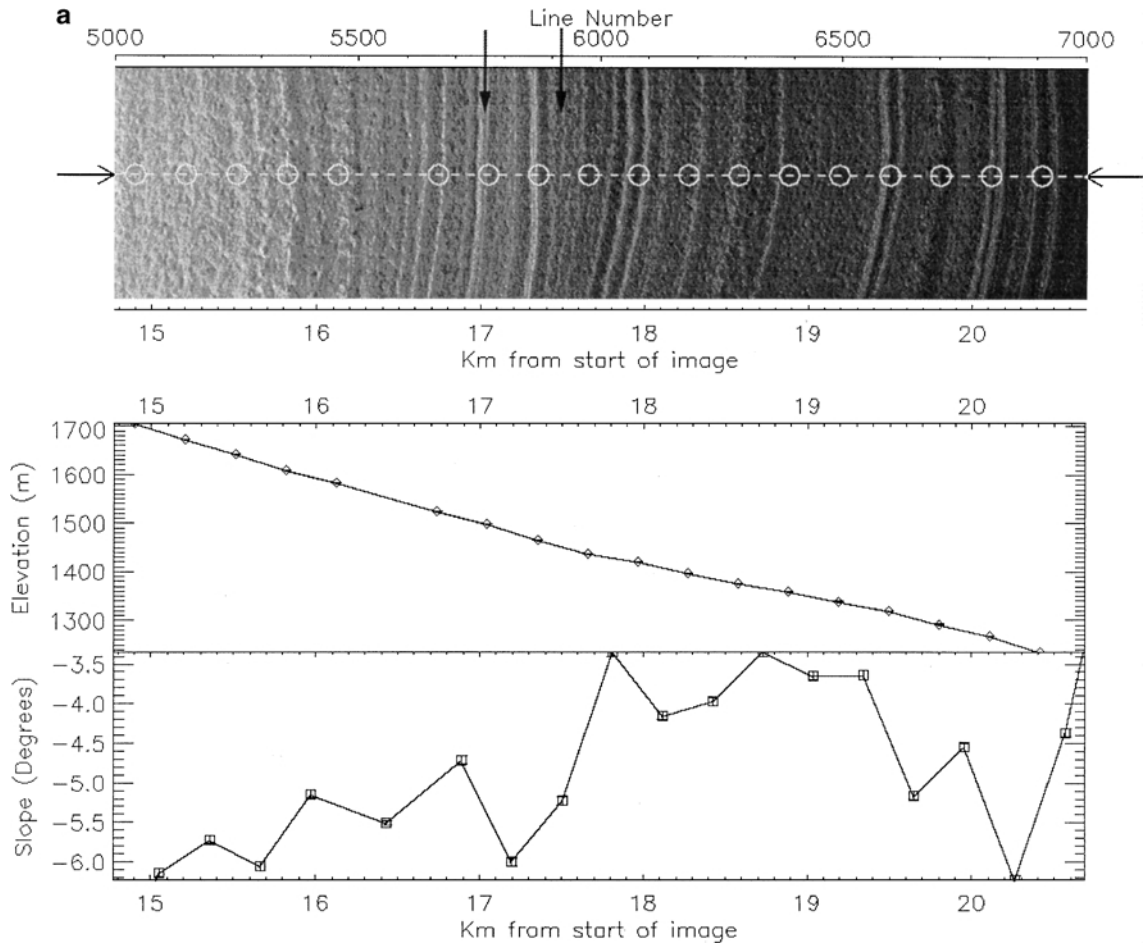


**FIG. 11a.** MOLA trace of m0305646 showing elevation and slope profiles across a portion of the image; illumination is from the upper right in this orientation. The resolution is 2.8 m/pixel and the solar elevation angle is  $11^\circ$ . The arrows point to a thin bright layer between two darker layers and a thin dark layer between two bright layers. Both layers exhibit a horizontal projection of about 10 m. The *average* slope there is about  $5.3^\circ$ . As illustrated in Fig. 11b, we estimate the actual thickness of such a thin layer in the range 1–4 m.

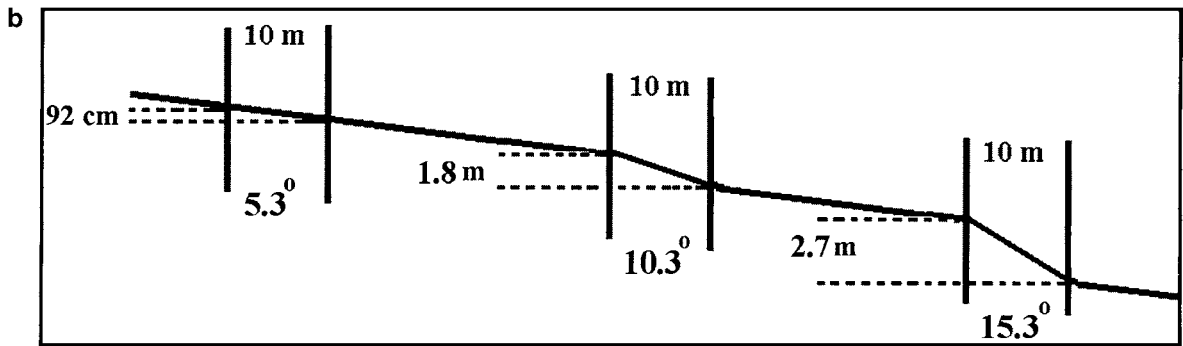


**FIG. 11b.** As illustrated above, if either thin layer were exposed smoothly parallel to that average slope, the thickness would be about 92 cm. If, on the other hand, the exposed bed outcrop exhibited an additional  $5^\circ$  slope toward the sun, then the thickness would be about 1.8 m. An excess outcrop slope of  $10^\circ$  would yield a thickness of 2.7 m and  $15^\circ$  would correspond to 3.7 m. Due to seasonal frost coverage at the time this image was acquired, we presume that any intrinsic albedo variations are covered and that only slope variations were manifest in the layering. If the frost-covered surface obeyed Lambert scattering, then the outcrop of the (relatively) dark layer probably is most nearly horizontal and the outcrop of the (relatively) bright layer probably slopes more steeply toward the sun. Accordingly, the image suggests to us a minimum layer thickness of 1–4 m, within a stack of layers with average layer thickness around 10 m.

what appears to be a local unconformity but could also be explained as a topographic bench. The MOLA profile is not located close enough to provide a clear answer. Local breaks in the sedimentary record have been reported in the NPLD and interpreted to indicate that the deposition process was discontinuous (Howard *et al.* 1982a, Thomas *et al.* 1992). Alternatively, local deformation there may have created local erosional surfaces which subsequent regional deposition overlapped. Using the higher resolution MOC NA images, it will be important now to check also for subhorizontal faulting in the NPLD as an alternative explanation for vertical breaks observed in the strata, such as appears to be the case in Fig. 10 in this SPLD study.

Figure 10 especially and Fig. 13a display a somewhat repetitive sequence of layering, especially in the lower portion, suggesting a similarly rhythmic variation in environmental conditions. Rhythmic deposition in the martian polar environment is strongly suggestive of climate modulation, a feature hypothesized by Cutts and Lewis (1982). As more complete stratigraphic records are unraveled, the extraction of a discernable climate signature within the overall array of depositional processes will be of great importance to the global history of Mars. We plan the systematic exploitation of the stratigraphic record available throughout the SPLD.

## 5. EVIDENCE OF DEFORMATION

Large-scale slumping associated with the gravitational stresses created by the bounding scarp is suggested first by the somewhat scalloped northern edge of the Ultimi lobe, and secondly

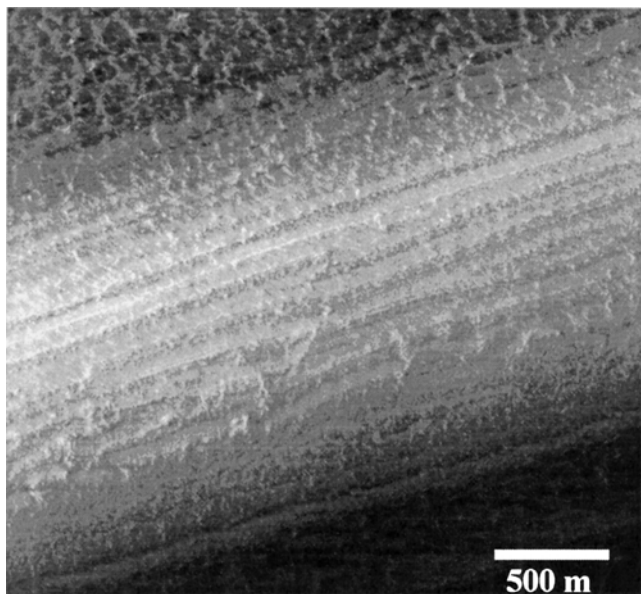


**FIG. 9.** A portion of MOC NA frame m0306702 at 73°S, 225°W. Taken at  $L_s = 181.8^\circ$ ; resolution = 4.3 m/pixel; illumination is from the lower right at 12° solar elevation. One group of layers appears disrupted, suggestive of intralayer deformation and possible incipient bedding plane faulting. The maximum slope across this exposed 700-m-thick section is approximately 23°.



**FIG. 10.** A portion of MOC NA frame m0302811 at 73°S, 224°W. Taken at  $L_s = 170.9^\circ$ ; resolution = 2.0 m/pixel. Note the somewhat repetitive sequence of layering, especially in the lower portion, implying similarly rhythmic variation in environmental depositional conditions. Also evident in the middle of the image (see arrows) is a subhorizontal break representing a lost section (and lost time), either an erosional unconformity or, more likely, subhorizontal faulting.

by the linear surface depressions oriented parallel to that scarp, as evident in Fig. 14. This interpretation is strengthened by the MOLA trace in Fig. 15, which displays a break in slope denoted by an arrow where it crosses one of those linear features, consistent with a small southward back rotation as would be expected for an incipient slump.

As mentioned above in Section 4, we think the most likely explanation for the abrupt break in the section designated by the arrows in Fig. 10 is subhorizontal faulting, not an erosional unconformity like those suggested for the NPLD (Howard *et al.* 1982b). An unconformity would be expected to exhibit beds parallel to the unconformity immediately above it, which does not appear to be the case. Also, intralayer deformation is apparent



**FIG. 13a.** A portion of MOC NA frame m0402455 at 73°S, 213°W.  $L_s = 192.4^\circ$ ; resolution = 3.6 m/pixel. A dramatic example of brittle fracture is to the left of center, exhibiting significant displacement, estimated to be about 415 m apparent horizontal and about 100 m apparent vertical. The sense of the apparent horizontal displacement is right lateral, but the actual fault displacement is uncertain. The fault trends obliquely to a bounding scarp at about 45° east of north. The fault appears to die out vertically or to terminate at an unconformity. A second possible fault trace is denoted with arrows. Profile A-A' is shown in Fig. 13c.

in Fig. 9 and is perhaps a related phenomenon resulting from localized shear in or close to the bedding plane. Thus, at least in these basal deposits, bedding plane faulting is suggested.

Even more surprising is the 400-m horizontal offset of layer outcrops evident in Fig. 13a. In Fig. 13b, an apparent vertical

displacement of about 100 m on a sloping surface of more than 16° can be estimated. We assume these layers also exhibit the 2–3° regional slope to the north measured from Figs. 8a and 8b. The dip of the fault plane, unfortunately, is unknown. Thus, the sense of displacement is ambiguous and could range from pure normal, to pure thrust, and to oblique strike-slip. Figure 13c illustrates conceptually how, for example, the observed outcrop offset could result from normal or thrust faulting.

The lack of an observable scarp on the upper surface of the SPLD in Figs. 13a and 13b makes it difficult to test these various structural interpretations, and it points as well to an ancient date of origin, prior to the erosion that formed the bounding scarp and exposed the fault trace. Inasmuch as no continuation of the fault into the underlying Hesperian beds can be recognized, the deformation most likely occurred during the time represented by the lowest portion of the SPLD now exposed in the scarp and ended before deposition of the higher layers. A plausible and important interpretation of this image is:

1. layers below the stratigraphic level marked by “A” in Fig. 13a are deposited;
2. normal, reverse, or oblique faulting event(s);
3. possible erosion of SPLD to stratigraphic level near “A”, removing scarp at upper surface;
4. deposition of material stratigraphically above “A”;
5. erosion of entire stack to expose layer outcrops and faults as seen today.

None of the possible fault orientations are easily reconciled with simple gravity failure parallel to the present retreating scarp because the trend of the fault is very different from the strike of the scarp. Connection with the current receding scarp is also ruled out by the evidence that the fault is a buried, ancient one. Nor is it likely we think that differential settling of the SPLD over topographic irregularities could provide an alternative explanation, but this cannot be completely ruled out. More likely, in our view, is that the timing, and perhaps the strike of this fault, is consistent with the deformation resulting from irregular frictional stresses created by basal sliding during the formation and outward translation of the SPLD “stack.” We have, so far, not recognized much evidence of brittle fracture higher in the SPLD, which is another tentative piece of evidence in support of basal sliding restricted to the basal contact of the SPLD with the underlying Hesperian deposits.

It will also be important in this regard to determine if brittle fracture is apparent or not elsewhere along the lowest contact of the SPLD with older units, where that lowest contact is well exposed with layers visible right at the contact.

## 6. MASS WASTING FEATURES

Figure 14 shows extensive mass wasting along the steepest portion of the bounding scarp in the area we have examined so far. The 39° average slope perpendicular to the scarp inferred

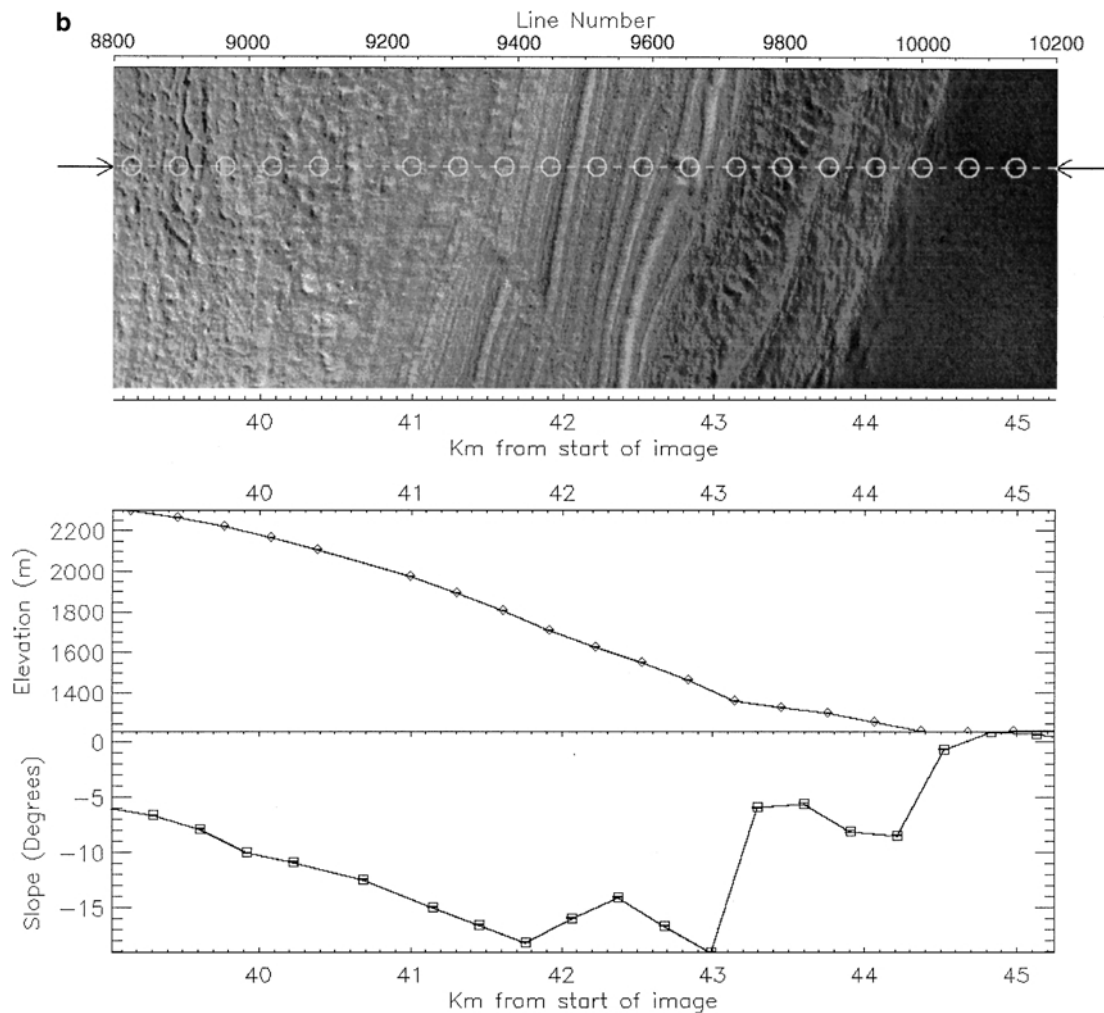


FIG. 13b. MOLA trace of a portion of frame m0402455 showing elevation and slope profiles, in conjunction with larger MOC image coverage.

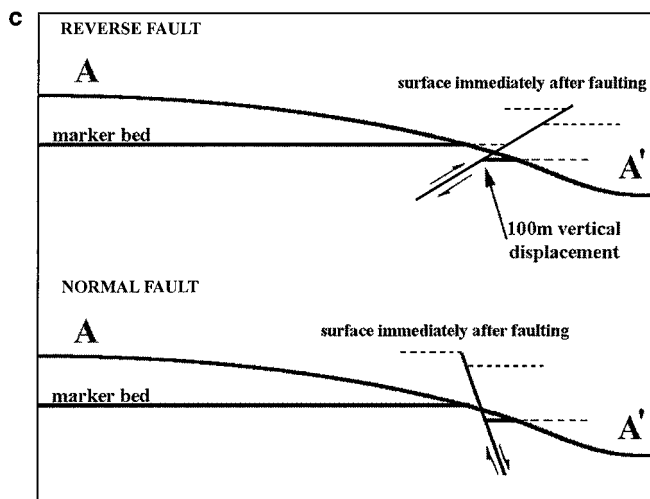


FIG. 13c. Schematic cross section A-A' (see Fig. 13a). Two possible alternative geometries which do not involve strike-slip motion for the fault trace in Fig. 13a are illustrated.

from the MOLA trace (that was generated in association with Fig. 15) implies locally steeper slopes. In any case, the average slope there is clearly above the angle of repose for loose, granular materials, suggesting some degree of competence for the strata. The MOLA profiles in Figs. 13b and 15 also show evidence for a shallower sloping zone at the base of the scarp, perhaps suggestive of a debris pile.

The bounding scarp generally is significantly steeper than Mangold *et al.* (2000) reported for a suspected ice scarp at Deuteronilus Mensae, 41°N, 342°W, using MOLA and DTM. Their reported slopes ranged from 9 to 25°, which they considered low in comparison with typical terrestrial scarp values. That might be regarded as an indication of ice flow there, but we do not consider that likely at our locality. Ice-rich deposits at 72°S will be sufficiently cold, even at high obliquities, that plastic flow would seem unlikely (Hofstadter and Murray 1990). A comprehensive rheological study of the bounding scarp, including the previously cited evidence for slumping, is underway by a subgroup of our team. From it we hope to place limits on

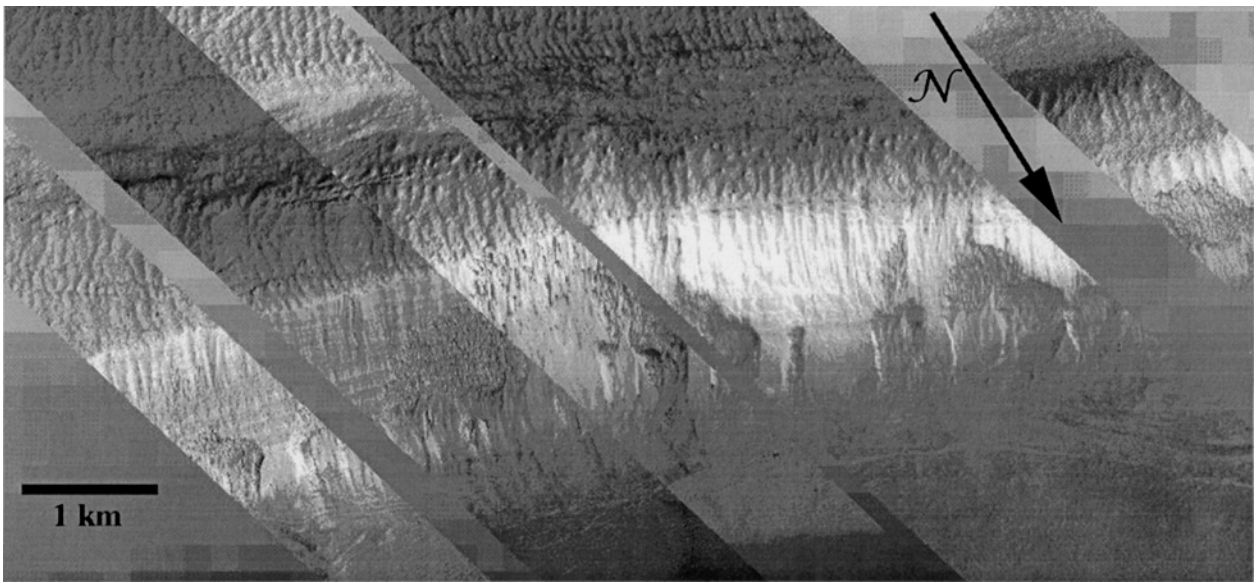


FIG. 14. Portions of MOC NA frames m1101401 (resolution = 2.2 m/pixel,  $L_s = 279.9^\circ$ ), m1200666 (resolution = 2.2 m/pixel,  $L_s = 296.3^\circ$ ), m0307394 (resolution = 3.6 m/pixel,  $L_s = 184.2^\circ$ ), m0201989 (resolution = 7.9 m/pixel,  $L_s = 155^\circ$ ), and m0302048 (resolution = 1.4 m/pixel,  $L_s = 169.24^\circ$ ) at approximately  $72^\circ\text{S}$ ,  $216^\circ\text{W}$ , as displayed in GIS. Illumination is from the lower right of each individual image in all cases. Note the complex landslides/mass movements occurring on this steep section of the bounding scarp.

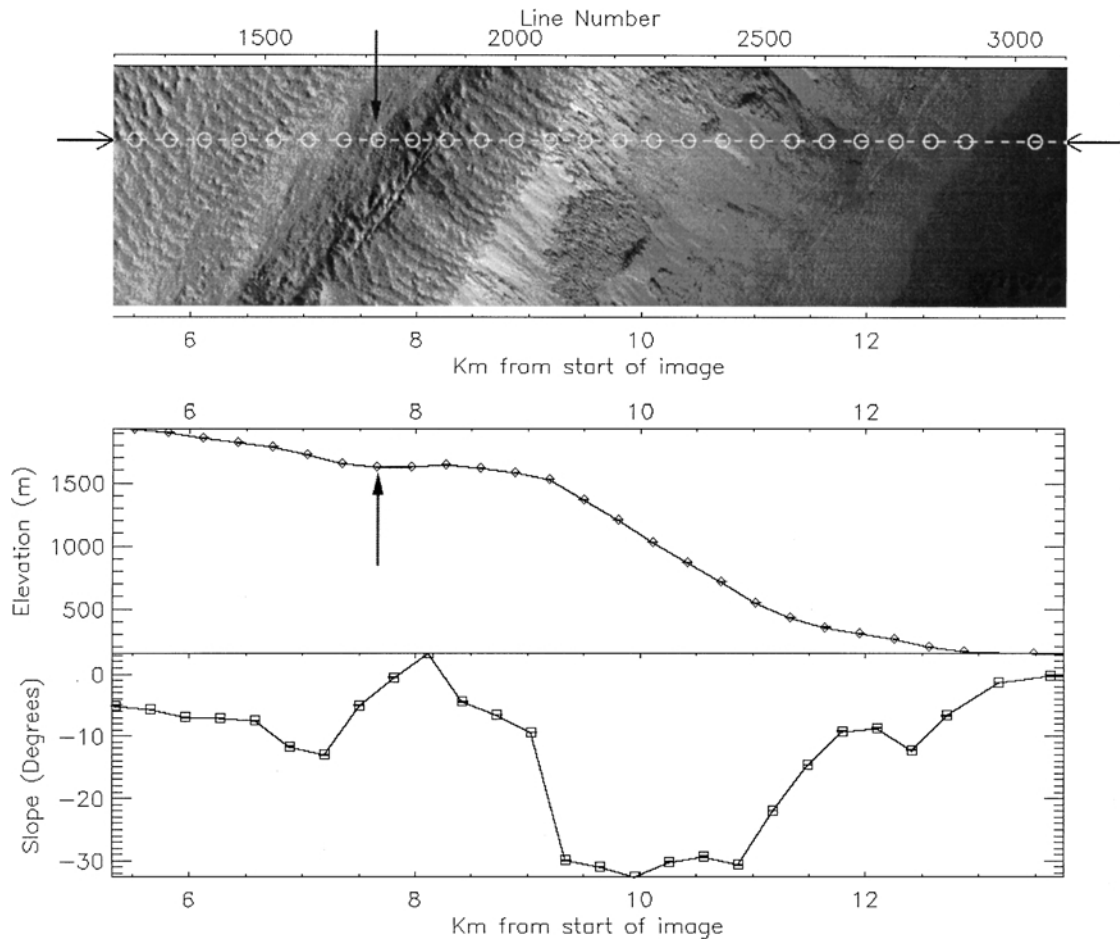


FIG. 15. MOLA track through MOC NA frame m0307394 (also shown in Fig. 14). The maximum average slope along the MOLA track is approximately  $32^\circ$  over an elevation change of 1 km. Taking into account the oblique orientation of the MOLA track to the scarp, we estimate the maximum scarp slope to be about  $39^\circ$ , with local portions steeper. The arrows mark a shallowing of the modest northward slope on the top residual layer which may reflect incipient large-scale slumping.

the material properties of at least the lower units of the SPLD, and to constrain mechanisms of scarp retreat.

## 7. DISCUSSION AND CONCLUSIONS

MGS imaging and topographic data provide important clues to the origin and history of the SPLD. The sharp and undisturbed contact of the SPLD with older units, and the lack of striations, argues against emplacement of the SPLD by glacial-like flow, at least in the Ultimi lobe region. Head (2000) proposed flow of SPLD at localities at the boundary of Chasma Australe and the Prometheus basin, as has Hartmann (2000) at the SPLD edge near 80°S and 240°W. Similarly, the broad range of scarp slopes, and the regular layering, seems inconsistent with differential ablation as a primary mechanism for evolving the shape and distribution of the SPLD. On the other hand, basal sliding is suggested by the unusual faulting in Figs. 13a–13c and may also be consistent with the possible bedding plane faulting of Figs. 9 and 10. Thus, our preliminary MGS observations support the concept of a rigid mass of primary sedimentary units comprising the SPLD, perhaps having deformed modestly by outward basal sliding or by settling, rather than dynamic, plastic deformation as some have speculated for the northern permanent cap.

However, it is important to note in any north–south comparison that we have investigated only the base of the SPLD located at a considerable distance from the younger dome-like topography in the central portion of the southern permanent cap. Indeed, the dissected plains of the Ultimi lobe and other peripheral portions of the SPLD are not well represented at all in the NPLD. Conceivably, different processes have operated in these two regimes, and perhaps also at each cap.

The retreat of the bounding scarp appears to be facilitated by surficial mass wasting on its steepest slopes, and probably also by larger-scale slumping. Indeed, slumping may contribute to the “scaloped” appearance in plan (Fig. 1). What is not so evident is the contribution to scarp retreat by ablation, as would be expected from solar heating of ice-rich materials. Hofstadter and Murray (1990) showed that an insulating layer of cemented fine clastics (which is inferred to weather out of the ice-clastic mixture composing the layered deposits) is required to prevent unreasonably rapid scarp retreat (see also Toon *et al.* 1980). Such an insulating coating is consistent with the unusually low thermal inertia estimates (Paige and Keegan 1994, Vasavada *et al.* 2000).

The layering details suggest a rich variation of changing physical attributes of the depositional, erosional, and diagenetic environment, not necessarily limited to just a simple cyclic variation in aeolian deposition driven by an astronomically modulated climate. Layers can be traced extensively, but they do evidence lateral changes in thickness, suggestive of locally varying depositional rates. No incontrovertible evidence of unconformities was recognized but some strong candidates exist. This should be an important element of continued study of the numerous exposed sections in the SPLD. Rhythmic bedding is apparent

in some horizons, suggesting a climate-modulated depositional signal at times. Inasmuch as ice appears to be a ubiquitous constituent of the SPLD, climatic conditions must have favored its formation and retention. However, we have not yet found a basis for eliminating hypothetical loess, or other periglacial environments, or volcanic contributions.

The population of craters is probably of impact origin, and is consistent with a 2 million year exposure age, although absolute time estimates are uncertain because of uncertainty in primary flux rates on Mars. Absence or removal of an otherwise common thin sedimentary blanket is implied for the cratered local areas we have discovered.

## ACKNOWLEDGMENTS

We gratefully acknowledge the assistance of the following individuals: Tammy Becker, USGS, for help with ISIS; Trent Hare, USGS, for assistance in development and use of a Mars Polar Stereographic GIS; Anton Ivanov and Scott Anderson of JPL for assistance in the collocation of MOLA traces and MOC NA images. Our access to and use of MOLA data was facilitated by the current, user-friendly MOLA team website. We thank the following for preliminary manuscript review: Arden Albee, Caltech; R. Ashwin Vasavada, Caltech; Anton Ivanov, JPL; Asmin Pathare, UCLA; and especially Jeffrey Plaut and James Cutts of JPL for their detailed and very helpful formal reviews.

## REFERENCES

- Blasius, K. R., J. A. Cutts, and A. D. Howard 1982. Topography and stratigraphy of martian polar layered deposits. *Icarus* **50**, 140–160.
- Condit, C., and L. A. Soderblom 1978. *Geological map of the Mare Australe Area of Mars*. U.S. Geological Survey Miscellaneous Investigation Map I-1076.
- Cutts, J. A. 1973. Nature and origin of layered deposits of the martian polar regions. *J. Geophys. Res.* **78**, 4231–4249.
- Cutts, J. A., and B. H. Lewis 1982. Models of climatic cycles recorded in martian polar layered deposits. *Icarus* **50**, 216–244.
- Cutts, J. A., K. R. Blasius, G. A. Briggs, M. H. Carr, R. Greeley, and H. Masursky 1976. North polar region of Mars: Imaging results from Viking 2. *Science* **194**, 1329–1337.
- Dzurisin, D., and K. R. Blasius 1975. Topography of the polar layered deposits of Mars. *J. Geophys. Res.* **89**, 3286–3306.
- Farmer, C. B., D. W. Davies, and D. D. LaPorte 1976. Mars: Northern summer ice cap–water vapor observations from Viking 2. *Science* **194**, 1339–1341.
- Fisher, D. A. 2000. Internal layers in an “accublation” ice cap: A test for flow. *Icarus* **144**, 289–294.
- Hartmann, W. K., R. Strom, S. Weidenschilling, K. R. Blasius, A. Woronow, M. Dence, R. Grieve, J. Diaz, C. Chapman, E. Shoemaker, and K. Jones 1981. Chronology of planetary volcanism by comparative studies of planetary cratering. In *Basaltic Volcanism on the Terrestrial Planets*, pp. 1050–1129. Basaltic Volcanism Project, New York: Pergamon Press.
- Hartmann, W. K. 1999. Martian cratering VI: Crater count isochrones and evidence for recent volcanism from Mars Global Surveyor. *Meteorol. Planet. Sci.* **34**, 167–177.
- Hartmann, W. K. 2000. Polar terrain and youthful geological processes on Mars. Presented at *2nd International Conference on Mars Polar Science and Exploration*, Lunar Planet. Inst. Contrib. No. 1057.
- Head, J. W. 2000. Evidence for geologically recent lateral migration of volatile rich polar layered deposits. Presented at *2nd International Conference on Mars Polar Science and Exploration*, Lunar Planet. Inst. Contrib. No. 1057.

- Herkenhoff, K. E. 2001. *Geologic map of the MTM-85000 Quadrangle, Planum Australe region of Mars*. U.S. Geological Survey Miscellaneous Investigations Series Map I-2686, in press.
- Herkenhoff, K. E., and R. L. Kirk 2000. Topography and stratigraphy of the polar layered deposits on Mars. Presented at *2nd International Conference on Mars Polar Science and Exploration*, Lunar Planet. Inst. Contrib. No. 1057.
- Herkenhoff, K. E., and R. L. Kirk 2001. MOC Photoclinometry of the polar layered deposits on Mars. *Lunar Planet. Sci.* **32**, 1129 (abstract); CD-ROM, Lunar Planet. Inst., Houston.
- Herkenhoff, K. E., and J. J. Plaut 2000. Surface ages and resurfacing rates of the polar layered deposits on Mars. *Icarus* **144**, 243–253.
- Hofstadter, M. D., and B. C. Murray 1990. Ice sublimation and rheology: Implications for the martian polar layered deposits. *Icarus* **84**, 352–361.
- Howard, A. D., K. R. Blasius, and J. A. Cutts 1982a. Photoclinometric determination of the topography of the martian north polar cap. *Icarus* **50**, 245–258.
- Howard, A. D., J. A. Cutts, and K. R. Blasius 1982b. Stratigraphic relationships within martian polar cap deposits. *Icarus* **50**, 161–215.
- Ivanov, A. B., and D. O. Muhleman 2000a. The role of the sublimation for the formation of the northern ice cap: Results from the Mars Orbiter Laser Altimeter. *Icarus* **144**, 436–448.
- Ivanov, A. B., and D. O. Muhleman 2000b. Topography of the north and south polar ice caps on Mars: Analysis of shape and troughs with a sublimation model. Presented at *2nd International Conference on Mars Polar Science and Exploration*, Lunar Planet. Inst. Contrib. No. 1057.
- Kieffer, H. H. 1979. Mars south polar spring and summer temperatures: A residual CO<sub>2</sub> frost. *J. Geophys. Res.* **84**, 8263–8288.
- Leighton, R. B., and B. C. Murray 1966. Behavior of carbon dioxide and other volatiles on Mars. *Science* **153**, 136–144.
- Malin, M. C., and K. S. Edgett 2000. The Mars Surveyor 1998 landing zone: Searching for Mars Polar Lander in high resolution MOC images. Presented at *2nd International Conference on Mars Polar Science and Exploration*, Lunar Planet. Inst. Contrib. No. 1057.
- Mangold, N., D. Baratoux, and V. Frey 2000. Slope analysis of scarps in Deuteronilus Mensae from MOLA data and Viking D.E.M.: Evidence for landslides controlled by ground ice. Presented at *2nd International Conference on Mars Polar Science and Exploration*, Lunar Planet. Inst. Contrib. No. 1057.
- Murray, B. C., L. A. Soderblom, J. A. Cutts, R. P. Sharp, D. J. Milton, and R. B. Leighton 1972. Geological framework of the south polar region of Mars. *Icarus* **17**, 328–345.
- Murray, B. C., W. R. Ward, and S. C. Yeung 1973. Periodic insolation variations on Mars. *Science* **180**, 638–640.
- Neukum, G., and B. A. Ivanov 2001. Crater production function for Mars. *Lunar Planet. Sci.* **32**, 1757 (abstract).
- Paige, D. A., K. E. Herkenhoff, and B. C. Murray 1990. Mariner 9 observations of the south polar cap of Mars: Evidence for residual CO<sub>2</sub> frost. *J. Geophys. Res.* **95**, 1315–1335.
- Paige, D. A., and K. D. Keegan 1994. Thermal and albedo mapping of the polar regions of Mars using Viking thermal mapper observations: 2. South polar region. *J. Geophys. Res.* **99**, 25,993–36,031.
- Plaut, J. J., R. Kahn, E. A. Guinness, and R. E. Arvidson 1988. Accumulation of sedimentary debris in the south polar region of Mars and implications for climate history. *Icarus* **75**, 357–377.
- Schenk, P. M., and J. M. Moore 1999. South polar cap and layered deposits of Mars: High-resolution stereo topographic and geologic mapping. *Lunar Planet. Sci.* **30**, 1819 (abstract); CD-ROM.
- Sharp, R. P. 1973. Mars: South polar pits and etched terrain. *Icarus* **78**, 4222–4230.
- Shoemaker, E. M. 1965. *Preliminary Analysis of the Fine Structure of the Lunar Surface*. Rep. 32-700, Jet Propulsion Laboratory, Pasadena.
- Shoemaker, E. M., and E. F. Helin 1977. Populations of planet-crossing asteroids and the relationship of Apollo objects to main belt asteroids and comets. In *Comets, Asteroids, Meteorites*, (A. H. Delsemme, Ed.), pp. 301–336. Univ. of Toledo Press, Toledo.
- Smith, D. E., and 18 colleagues 1999. The global topography of Mars and implications for surface evolution. *Science* **284**, 1495–1502.
- Soderblom, L. A. 1977. Historical variations in the density and distribution of impacting debris in the inner Solar System: Evidence from planetary imaging. In *Impact and Explosion Cratering* (D. J. Roddy, R. O. Pepin, and R. B. Merrill, Eds.), pp. 629–633. Pergamon, Elmsford, NY.
- Soderblom, L. A., M. C. Malin, J. A. Cutts, and B. C. Murray 1973. Mariner 9 observations of the surface of Mars in the north polar region. *J. Geophys. Res.* **78**, 4197–4210.
- Soderblom, L., C. Condit, R. West, B. Herman, and T. Kreidler 1974. Martian planet wide crater distributions: Implications for geologic history and surface processes. *Icarus* **22**, 239–263.
- Tanaka, K. L. 1986. The stratigraphy of Mars. *J. Geophys. Res.* **91**, E139–E158.
- Tanaka, K. L., and E. M. Kolb 2001. Geologic history of the polar regions of Mars: I. Noachian and Hesperian Periods. *Icarus* **154**, 3–21.
- Tanaka, K. L., and D. H. Scott 1987. *Geologic Map of the Polar Regions of Mars*. U.S. Geological Survey Miscellaneous Investigation Map I-1802-C.
- Tanaka, K. L., P. H. Schultz, and K. E. Herkenhoff 2000. Stratigraphy and topography of McMurdo crater area, Planum Australe Mars: Implications for resurfacing history and porous character of the south polar layered deposits. Presented at *2nd International Conference on Mars Polar Science and Exploration*, Lunar Planet. Inst. Contrib. No. 1057.
- Thomas, P. C., and C. Weitz 1989. Dune sand materials and polar layered deposits on Mars. *Icarus* **81**, 185–215.
- Thomas, P., S. Squyres, K. Herkenhoff, A. Howard, and B. Murray 1992. Polar deposits of Mars. In *Mars* (H. H. Kieffer, B. M. Jakosky, C. W. Snyder, and M. S. Matthews, Eds.), pp. 767–795. Univ. of Arizona Press, Tucson.
- Toon, O. B., J. B. Pollack, W. Ward, J. A. Burns, and K. Bilski 1980. The astronomical theory of climatic change on Mars. *Icarus* **44**, 552–607.
- Touma, J., and J. Wisdom 1993. The chaotic obliquity of Mars. *Science* **259**, 1294–1296.
- Vasavada, A. R., J.-P. Williams, D. A. Paige, K. E. Herkenhoff, N. T. Bridges, R. Greeley, B. C. Murray, D. S. Bass, and K. S. McBride 2000. Surface properties of Mars' polar layered deposits and polar landing sites. *J. Geophys. Res.* **105**, 6961–6969.
- Ward, W. R. 1974. Climatic variations on Mars. 1. Astronomical theory of insolation. *J. Geophys. Res.* **79**, 3375–3386.
- Ward, W. R. 1979. Present obliquity oscillations of Mars: Fourth-order accuracy in orbital  $e$  and  $I$ . *J. Geophys. Res.* **84**, 237–241.
- Zuber, M. T., D. E. Smith, G. A. Neumann, and F. G. Lemoine 2000. Structure and dynamics of the polar regions of Mars from MGS topography and gravity. Presented at *2nd International Conference on Mars Polar Science and Exploration*, Lunar Planet. Inst. Contrib. No. 1057.